PAI-1–regulated extracellular proteolysis governs senescence and survival in *Klotho* mice

Mesut Eren[a], Amanda E. Boe[a,b], Sheila B. Murphy[a,b], Aaron T. Place[a,b], Varun Nagpal[a,b], Luisa Morales-Nebreda[a], Daniela Urich[a], Susan E. Quaggin[a,b], G. R. Scott Budinger[a], Gökhan M. Mutlu[a], Toshio Miyata[c], and Douglas E. Vaughan[a,b,1]

[a]Department of Medicine and [b]Feinberg Cardiovascular Research Institute, Northwestern University Feinberg School of Medicine, Chicago, IL 60611; and [c]United Centers for Advanced Research and Translational Medicine, Tohoku University Graduate School of Medicine, Miyagi 980-8575, Japan

Edited* by David Ginsburg, University of Michigan Medical School, Ann Arbor, MI, and approved April 2, 2014 (received for review November 25, 2013)

Cellular senescence restricts the proliferative capacity of cells and is accompanied by the production of several proteins, collectively termed the "senescence-messaging secretome" (SMS). As senescent cells accumulate in tissue, local effects of the SMS have been hypothesized to disrupt tissue regenerative capacity. *Klotho* functions as an aging-suppressor gene, and *Klotho*-deficient (*kl/kl*) mice exhibit an accelerated aging-like phenotype that includes a truncated lifespan, arteriosclerosis, and emphysema. Because plasminogen activator inhibitor-1 (PAI-1), a serine protease inhibitor (SERPIN), is elevated in *kl/kl* mice and is a critical determinant of replicative senescence in vitro, we hypothesized that a reduction in extracellular proteolytic activity contributes to the accelerated aging-like phenotype of *kl/kl* mice. Here we show that PAI-1 deficiency retards the development of senescence and protects organ structure and function while prolonging the lifespan of *kl/kl* mice. These findings indicate that a SERPIN-regulated cell-nonautonomous proteolytic cascade is a critical determinant of senescence in vivo.

FGF23 | IGFBP3 | IL-6 | TM5441

Advanced age contributes to the development of frailty and disease in humans, but the fundamental mechanisms that drive physiological aging are incompletely understood (1, 2). Cellular senescence, which halts the proliferative capacity of cells, is associated with the manifestation of the senescence-associated secretory phenotype (3) and the production and secretion of a distinct set of proteins (2, 4), including insulin-like growth factor-binding proteins (IGFBPs), interleukins (ILs), transforming growth factor type β (TGF-β), and plasminogen activator inhibitor-1 (PAI-1) (5), collectively termed the "senescence-messaging secretome" (SMS) (6). In addition to this pattern of protein production and secretion, senescent cells display a distinctive morphology, and can be identified by increased expression of senescence-associated β-galactosidase (7). The tumor suppressor and proapoptotic protein p53 plays a central role in inducing replicative senescence by regulating the transcription of genes involved in cell cycle arrest and apoptosis, including the cyclin-dependent kinase inhibitors $p16^{Ink4a}$ and p21 (8). Senescence can be triggered by a number of factors, including DNA damage (9), oncogene induction (10), and oxidative stress (11). Although the relationship between cellular senescence and physiological aging remains an area of intense investigation, it is becoming increasingly evident that the two processes are fundamentally linked. Senescent cells accumulate in aging tissues and have been hypothesized to disrupt tissue regeneration, which may reflect cell-nonautonomous effects of the SMS (6).

In the last decade, numerous examples of genetically modified mice with phenotypes reminiscent of human aging have been described and investigated. These include the $BubR1^{H/H}$ progeroid (12) and *Klotho*-deficient (*kl/kl*) mice (13). $BubR1^{H/H}$ progeroid mice exhibit an age-dependent increase in the expression levels of PAI-1 in numerous locations, including white adipose tissue, skeletal muscle, and the eye (12). $BubR1^{H/H}$ mice have a shortened average lifespan (24 wk) and develop various aging-like phenotypic abnormalities, including sarcopenia, cataracts, arterial stiffening, and impaired wound healing (14). Klotho functions as an aging-suppressor protein by impeding the development of senescence in vitro and in vivo through inhibition of the Wnt (15), TGF-β (16), and IGF1 signaling pathways (17). Thus, *kl/kl* mice exhibit a rapidly progressive phenotype after weaning that includes a truncated lifespan (8–12 wk), renal sclerosis, arteriosclerosis, emphysema, and osteoporosis (13). Membrane-bound Klotho forms a heterodimer with fibroblast growth factor (FGF) receptors (FGFRs) generating a high-affinity receptor for FGF23. Signals transduced by FGF23 via the Klotho–FGFR complex inhibit 1,25-$(OH)_2$ vitamin D_3 and parathyroid hormone synthesis and promote renal phosphate excretion. *kl/kl* mice exhibit a remarkable increase in plasma levels of FGF23, as well as significant increases in serum levels of calcium, phosphate, vitamin D_3, and creatinine (13). Interestingly, *kl/kl* mice also have an age-dependent increase in plasma PAI-1 levels as well as increased PAI-1 expression in a number of tissues including kidney, aorta, and heart (18). Because PAI-1 is necessary and sufficient to induce replicative senescence in vitro downstream of p53 (19) and is markedly increased in *kl/kl* mice, we hypothesized that PAI-1 is a critical determinant of the phenotypic abnormalities developed by *kl/kl* mice. Here we examined the impact of PAI-1 on senescence and physiological aging in vivo by breeding *kl/kl* and PAI-1–deficient ($pai\text{-}1^{-/-}$) mice to generate *kl/kl* mice with partial ($kl/klpai\text{-}1^{+/-}$) or complete ($kl/klpai\text{-}1^{-/-}$) PAI-1 deficiency.

Results

PAI-1 Deficiency Prolongs the Survival of *kl/kl* Mice. We systematically monitored the effect of PAI-1 deficiency on the growth, vigor, and survival of littermate *kl/kl* ($n = 26$), $kl/klpai\text{-}1^{+/-}$ ($n = 39$), $kl/klpai\text{-}1^{-/-}$ ($n = 25$), and WT ($n = 16$) mice (Fig. 1) all in the

Significance

Plasminogen activator inhibitor-1 (PAI-1) is an essential mediator of cellular senescence in vitro and is one of the biochemical fingerprints of senescence in vivo. *Klotho*-deficient (*kl/kl*) mice display a complex phenotype reminiscent of human aging and exhibit age-dependent increases in PAI-1 in tissues and in plasma. Thus, we hypothesized that PAI-1 contributes to the aging-like phenotype of *kl/kl* mice. We observed that either genetic deficiency or pharmacological inhibition of PAI-1 in *kl/kl* mice was associated with reduced evidence of senescence, preserved organ structure and function, and a fourfold increase in median lifespan. These findings indicate that PAI-1 is a critical mediator of senescence in vivo and defines a novel target for the prevention and treatment of age-related disorders in man.

Author contributions: M.E. and D.E.V. designed research; M.E., A.E.B., S.B.M., A.T.P., V.N., L.M.-N., and D.U. performed research; T.M. contributed new reagents/analytic tools; M.E., S.E.Q., G.R.S.B., G.M.M., and D.E.V. analyzed data; and M.E. and D.E.V. wrote the paper.

The authors declare no conflict of interest.

*This Direct Submission article had a prearranged editor.

[1]To whom correspondence should be addressed. E-mail: d-vaughan@northwestern.edu.

This article contains supporting information online at www.pnas.org/lookup/suppl/doi:10.1073/pnas.1321942111/-/DCSupplemental.

same genetic background (75% C57BL/6J, 25% C3J). We observed that either partial or complete absence of PAI-1 prolonged the survival of *kl/kl* mice. Log-rank analysis indicated that the survival curves for the WT, *kl/kl*, *kl/klpai-1*$^{+/-}$, and *kl/klpai-1*$^{-/-}$ mice differed significantly ($P < 0.0001$). The median survival of *kl/kl* mice was 58 d, and this value increased with PAI-1 deficiency: 2.8-fold (163 d) in *kl/klpai-1*$^{+/-}$ mice and 4.2-fold (246 d) in *kl/klpai-1*$^{-/-}$ mice. Whereas all of the *kl/kl* mice died within 120 d, 65% of *kl/klpai-1*$^{+/-}$ and 82% of *kl/klpai-1*$^{-/-}$ mice were alive beyond 120 d. Although median survival indicates a dose–response relationship between genotype and mortality ($P = 0.0002$ by log-rank test for trend), the mean lifespan increased similarly in *kl/klpai-1*$^{+/-}$ (250 ± 169 d) and *kl/klpai-1*$^{-/-}$ (254 ± 123 d) mice (mean ± SD), corresponding to 4.2- and 4.5-fold increases, respectively. Furthermore, we achieved a similar prolongation of lifespan in *kl/kl* mice ($n = 11$) (Fig. 1*B*) by the administration of an orally active small-molecule PAI-1 antagonist, TM5441, whose pharmacokinetic properties, toxicity, and specificity have been described recently (20). In contrast with the inconsistent effects based on sex of a low phosphate diet on survival in *kl/kl* mice (21), both males and females appear to benefit from complete PAI-1 deficiency. However, survival of *kl/klpai-1*$^{+/-}$ females ($n = 19$) was not as long as that of males ($n = 20$) of the same genotype (median survival 121 d vs. 315 d, mean lifespan 208 ± 151 d vs. 285 ± 182, respectively; $P = 0.16$). Nevertheless, *kl/klpai-1*$^{+/-}$ females do live longer than *kl/kl* females ($n = 14$) (median survival 121 d vs. 58 d, mean lifespan 208 ± 151 d vs. 57 ± 18, respectively; $P = 0.0004$) (Fig. S1). This improvement in survival was also associated with evidence of increased overall vigor and health, as *kl/klpai-1*$^{-/-}$ mice exhibited near-normal weight gain over time (Fig. 1 *A* and *C*) and spontaneous physical activity (Fig. 1*D*).

PAI-1 Deficiency Normalizes Senescence and Telomere Length in *kl/kl* Mice. To characterize the extent of senescence in *kl/kl* mice and how PAI-1 deficiency affects it, plasma levels of the SMS factors IGFBP-3 and IL-6, and telomere length were measured in liver, aorta, tail, and kidney tissue. We observed that *kl/kl* mice had increased levels of IGFBP-3 (Fig. 2*A*) compared with WT mice ($P = 0.02$). With partial ($P = 0.03$ vs. *kl/kl* mice) or complete PAI-1 deficiency ($P = 0.02$ vs. *kl/kl* mice), IGFBP-3 levels did not significantly differ from those seen in WT mice. Similarly, we found that compared with levels in WT mice, *kl/kl* mice had a 13-fold increase ($P = 0.02$) in plasma levels of proinflammatory cytokine IL-6, which functions in the acquisition of the senescent phenotype in vitro (Fig. 2*B*). Compared with *kl/kl* mice, IL-6 levels were reduced by 79% in *kl/klpai-1*$^{+/-}$ ($P = 0.03$) and 83% in *kl/klpai-1*$^{-/-}$ ($P = 0.0001$) mice. These observations suggest that the elevated PAI-1 levels in *kl/kl* mice are a dominant factor in contributing to increases in plasma IGFBP-3 and IL-6 and further augment the senescent phenotype in these mice.

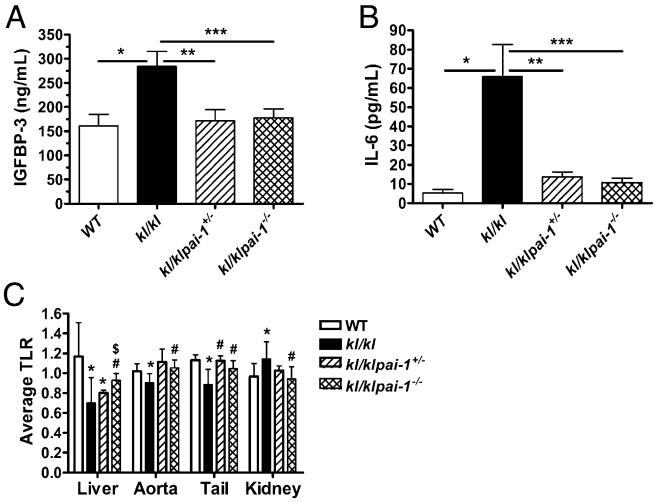

Fig. 2. Effect of PAI-1 deficiency on plasma levels of SMS factors and ATLR in various tissues from age-matched littermate *Klotho* mice. (*A*) Determination of IGFBP-3 levels in plasma samples ($n = 6$ per group). *$P = 0.02$, **$P = 0.03$, and ***$P = 0.02$. (*B*) Quantitation of circulating IL-6 levels ($n = 6$ to 14). *$P = 0.02$, **$P = 0.03$, and ***$P = 0.0001$. (*C*) Quantitation of ATLR by qRT-PCR in liver, aorta, tail, and kidney tissue ($n = 6$ to 14). *$P < 0.05$ compared with WT, $^{\#}P < 0.05$ compared with *kl/kl*, and $^{\$}P < 0.05$ compared with *kl/klpai-1*$^{+/-}$. Data are plotted as mean ± SD.

Although elevated plasma levels of SMS components may reflect systemic senescence, they are nonspecific in nature and do not provide precise identification of which tissues are actually senescent. To address this limitation, telomere length was determined in several different tissues. Liver, aorta, and tail tissue samples from *kl/kl* mice displayed moderate but significant decreases in the average telomere length ratio (ATLR), whereas renal tissue had 16% longer ATLRs compared with those of WT animals (Fig. 2*C*). In contrast, ATLRs of liver and tail tissues from *kl/klpai-1*$^{+/-}$ and liver, aorta, and tail, tissues from *kl/klpai-1*$^{-/-}$ mice were significantly longer than those of *kl/kl* mice. These findings indicate that PAI-1 deficiency provides partial protection of telomere integrity in numerous tissues. The anomalous

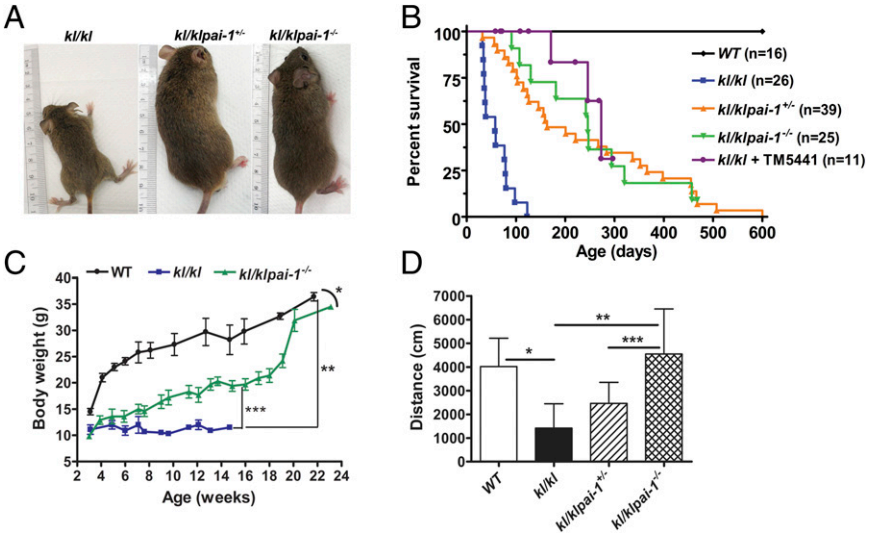

Fig. 1. Effects of PAI-1 deficiency in *Klotho* mice. (*A*) Size and appearance of 8-wk-old littermate mice. (*B*) Survival curve. Log-rank analysis showed that the survival curves for the WT, *kl/kl*, *kl/klpai-1*$^{+/-}$, and *kl/klpai-1*$^{-/-}$ mice differed significantly ($P < 0.0001$). (*C*) Bodyweight measurements starting from 3 wk of age. *$P = 0.002$, **$P = 0.0001$, and ***$P = 0.0003$. (*D*) Open field physical activity measurements recorded as distance traveled in 20 min in age-matched animals. *$P = 0.027$, **$P = 0.018$, and ***$P = 0.036$. Data are plotted as mean ± SD.

preservation of telomere length in renal tissue from *kl/kl* mice may reflect the lack of turnover in renal cells and the early induction of replicative senescence in the kidneys of *kl/kl* mice (22).

Because the kidneys are one of the most severely compromised organs in *kl/kl* mice, we also examined kidneys for biomarkers of senescence, including $p16^{Ink4a}$ and p21. We detected strong immunostaining for $p16^{Ink4a}$ localized in the nuclei of tubules in kidney tissues from *kl/kl* mice (Fig. 3), but not for p21. In contrast, kidney sections from *kl/klpai-1*$^{-/-}$ mice had only minimal evidence of $p16^{Ink4a}$ accumulation (Fig. 3). Quantitative real-time PCR (qRT-PCR) analysis showed that the relative expression of $p16^{Ink4a}$ in kidneys from *kl/kl* mice is 3.2-fold higher than that in WT mice ($P = 0.001$) (Fig. 3*E*). In *kl/klpai-1*$^{+/-}$ and *kl/klpai-1*$^{-/-}$ mice, $p16^{Ink4a}$ expression was reduced by 80% ($P = 0.04$) and 92% ($P = 0.0001$) compared with the *kl/kl* mice, respectively, and in *kl/klpai-1*$^{-/-}$ mice by 78% compared with the levels seen in WT animals ($P = 0.0001$).

Effect of PAI-1 Deficiency on the Biochemical Hallmarks of *kl/kl* Mice. In an effort to explain the effects of PAI-1 deficiency on the *kl/kl* phenotype, we measured plasma levels of factors that are biochemical hallmarks of *kl/kl* mice, including FGF23, vitamin D_3, calcium, phosphate, creatinine, and PAI-1 (Table 1). As expected, *kl/kl* mice displayed a more than 1,200-fold increase in FGF23 levels [$2.8 \times 10^5 \pm 1.4 \times 10^5$ pg/mL vs. 225 ± 65 pg/mL in WT mice ($P = 0.004$)], reflecting the loss of functioning receptors for FGF23. Both *kl/klpai-1*$^{+/-}$ and *kl/klpai-1*$^{-/-}$ mice exhibited a nearly 98% reduction in plasma FGF23 levels compared with *kl/kl* mice [$3.4 \times 10^3 \pm 2.1 \times 10^3$ pg/mL ($P < 0.0001$) and $3.9 \times 10^3 \pm 0.9 \times 10^3$ pg/mL ($P = 0.0001$), respectively]. Similarly, vitamin D_3 levels were reduced in *kl/klpai-1*$^{+/-}$ ($P = 0.032$) and *kl/klpai-1*$^{-/-}$ ($P = 0.0003$) mice compared with the levels in *kl/kl* mice. Interestingly, partial or complete PAI-1 deficiency had only a marginal impact on serum levels of calcium, phosphate, and creatinine in *kl/kl* mice. As expected, PAI-1 antigen was not detectable in plasma from *kl/klpai-1*$^{-/-}$ mice, and levels in *kl/klpai-1*$^{+/-}$ animals were reduced by nearly 50% compared with those from *kl/kl* mice ($P < 0.05$). In addition, PAI-1 expression levels were reduced in tissues from *kl/klpai-1*$^{+/-}$ mice compared with those of *kl/kl* mice (Fig. S2).

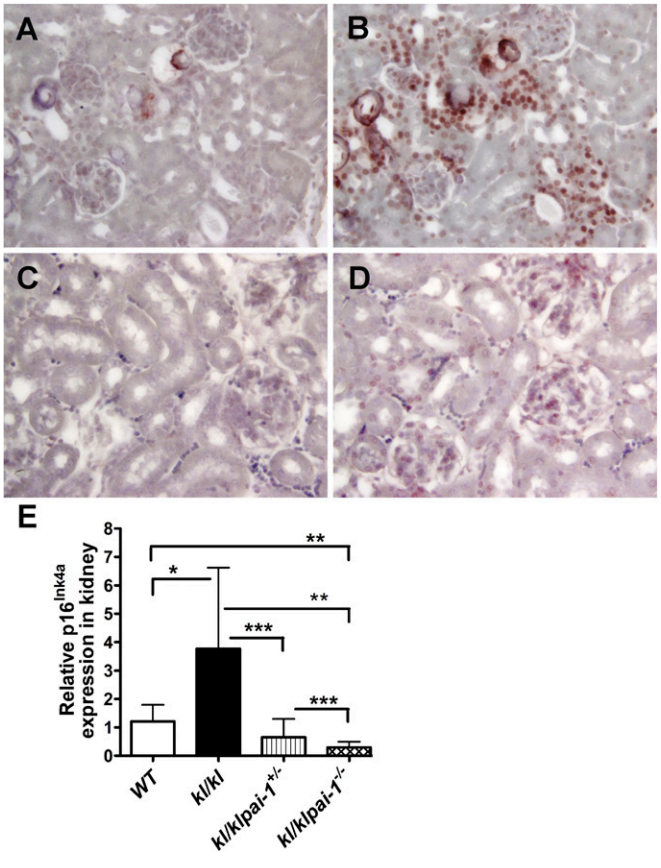

Fig. 3. Effect of PAI-1 deficiency on renal $p16^{Ink4a}$ expression in *Klotho*-deficient mice. (*A* and *C*) Control immunostaining of kidney sections from *kl/kl* and *kl/klpai-1*$^{-/-}$ mice, respectively, in the absence of the anti-$p16^{Ink4a}$ antibody. (*B* and *D*) Immunodetection of $p16^{Ink4a}$-positive cells in kidney sections from *kl/kl* and *kl/klpai-1*$^{-/-}$ mice, respectively. (*E*) Quantitation of relative $p16^{Ink4a}$ expression in the kidney. qRT-PCR analysis was performed on total RNA samples purified from WT ($n = 8$), *kl/kl* ($n = 6$), *kl/klpai-1*$^{+/-}$ ($n = 4$), and *kl/klpai-1*$^{-/-}$ ($n = 8$) kidneys. *$P = 0.001$, **$P = 0.0001$, and ***$P = 0.04$. Data are plotted as mean ± SD. (Magnification: *A–D*, 60×.)

PAI-1 Deficiency Preserves Organ Structure in *kl/kl* Mice. As reported previously, *kl/kl* mice develop emphysema that is characterized by a progressive, age-dependent enlargement of air spaces and associated alveolar destruction (Fig. 4) (23). Histological analysis of lung tissues from *kl/klpai-1*$^{+/-}$ and *kl/klpai-1*$^{-/-}$ (Fig. 4) mice showed that PAI-1 deficiency primarily prevents alveolar enlargement. Consistent with the preservation of pulmonary structural integrity, pulmonary function was also maintained with PAI-1 deficiency. We found that *kl/kl* mice had a 40% decrease in PaO_2 levels ($P = 0.018$) in arterial blood samples. Arterial oxygenation normalized with partial ($P = 0.05$) and complete ($P = 0.02$) PAI-1 deficiency in *kl/kl* mice (Fig. 4*E*). These results indicate that PAI-1 is an important contributor to the emphysematous changes observed in *kl/kl* mice.

Finally, we analyzed mice for evidence of ectopic calcification, which has been reported to increase with age in *kl/kl* mice. Whereas the age-matched WT littermate mice had no detectable calcification, we observed prominent calcium deposits in the kidneys of *kl/kl* mice (Fig. 5 *A* and *B*) ($P = 0.002$). However, analysis of kidneys from *kl/klpai-1*$^{+/-}$ (Fig. 5*C*) and *kl/klpai-1*$^{-/-}$ (Fig. 5*D*) mice showed that ectopic calcification areas were significantly reduced by 41% ($P = 0.03$) and 96% ($P < 0.0001$), respectively. To test the effect of PAI-1 deficiency on the impaired osteogenic signaling observed in *kl/kl* mice (24, 25), we measured the serum levels of aldosterone and alkaline phosphatase (ALP) activity (Table 1). Although aldosterone levels were significantly higher in *kl/kl* mice than that of WT animals, it was not altered significantly in *kl/klpai-1*$^{-/-}$ mice. Furthermore, we did not observe any difference in ALP activity among the mice groups studied here. This observation indicates that partial or complete loss of PAI-1 expression protects against age-induced ectopic calcification in *kl/kl* mice without altering serum levels of phosphate, calcium, ALP and aldosterone.

Discussion

PAI-1 is expressed in senescent cells and tissues, and is recognized as a primary component of the SMS. Most mammalian models of aging investigated thus far exhibit evidence of increased PAI-1 expression (12, 14). Furthermore, genetic or therapeutic interventions that prolong survival or reduce senescence in tissues in vivo are coincidentally associated with reductions in PAI-1. To our knowledge, this in vivo study is the first to investigate systematically the role of PAI-1 not only in the development of senescence, but also in the aging-like pathology of a mammal. The results from this study suggest that the onset of physiological aging can be delayed by modulating PAI-1, which subsequently prevents the nuclear accumulation of senescence marker $p16^{Ink4a}$ and maintains the structural and functional integrity of vital organs. Furthermore, the ability of a small-molecule PAI-1 antagonist to augment survival to a similar extent in *kl/kl* mice indicates that the observed effects are likely cell-nonautonomous. The protective effects of partial or complete PAI-1 deficiency are in agreement with previous work from our laboratory indicating that transgenic overexpression of

Table 1. Effects of PAI-1 deficiency on blood levels of the biochemical hallmarks of *klotho* mice

Circulating factors assayed	WT $n = 4$ to 5	*kl/kl* $n = 6$ to 9	*kl/klpai-1*$^{+/-}$ $n = 5$ to 6	*kl/klpai-1*$^{-/-}$ $n = 6$ to 10
Phosphate, mg/dL	7.7 ± 1.6	14.0 ± 2.8*	10.8 ± 2.6*	12.6 ± 2.7*
Calcium, mg/dL	7.9 ± 0.6	10.4 ± 0.9*	10.1 ± 1.2*	10.6 ± 0.8*
Creatinine, mg/dL	0.22 ± 0.11	0.31 ± 0.33	0.21 ± 0.11	0.18 ± 0.06
PAI-1, ng/mL	1.8 ± 0.4	45.2 ± 4.8*	24.3 ± 2.7*	0.0
FGF23, pg/mL	225 ± 65	295,657 ± 139,709*	3,924 ± 1,316*,#	3,795 ± 870*,#
Vitamin D_3, pg/mL	ND	1359 ± 145	698 ± 419#	314 ± 244#
Aldosterone, pg/mL	102 ± 20	160 ± 55*	ND	223 ± 96*
ALP, U/mL	20 ± 7	21 ± 6	17 ± 7	19 ± 5

ND, not determined.
*$P < 0.05$ compared with WT.
#$P < 0.05$ compared with *kl/kl*.

PAI-1 is sufficient to induce several aging-like phenotypic abnormalities, including age-dependent spontaneous coronary thrombosis, systemic amyloid deposition, and hair loss (26).

The normalization of FGF23 and vitamin D_3 levels in partial or complete PAI-1 knockout models strongly indicates that PAI-1 directly influences FGF23 signaling in *kl/kl* mice. Recent observations demonstrate that FGF23 is highly sensitive to cleavage by the serine protease furin, which is rapidly inhibited by PAI-1 (27, 28). In addition to FGF23, *kl/kl* mice have augmented expression of other furin substrates, including IGF1, TGF-β, MMP2, and MMP9 (29, 30). PAI-1 is known to regulate the proteolytic activation and/or clearance of many of these proteins. The precise identity and function of other proteases that are inhibited by PAI-1 and that contribute to the *Klotho* phenotype merits further investigation.

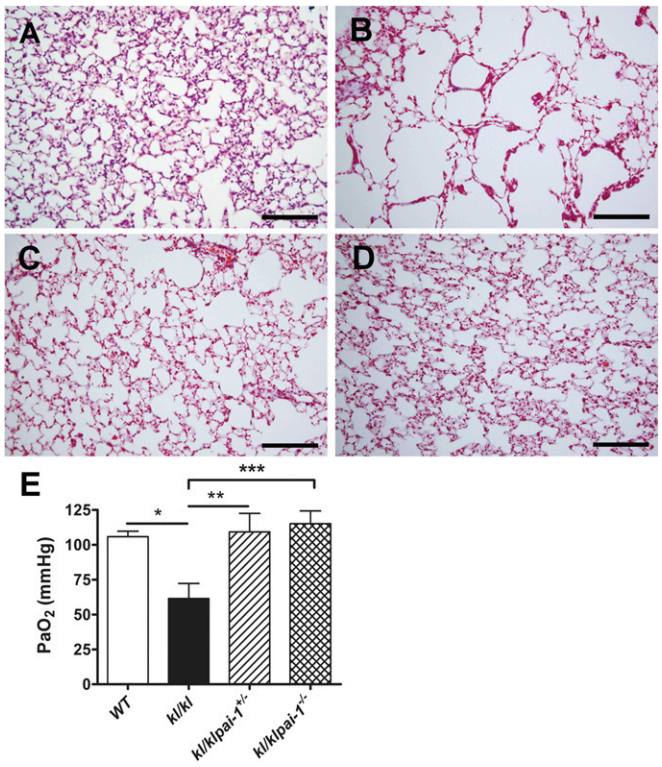

Fig. 4. Effects of PAI-1 deficiency on lung morphology and function. Masson's trichrome staining of lung sections in (*A*) WT, (*B*) *kl/kl*, (*C*) *kl/klpai-1*$^{+/-}$, and (*D*) *kl/klpai-1*$^{-/-}$ mice. (Scale bars: 150 μm.) (*E*) Partial pressure of oxygen (PaO_2) measurements in arterial blood ($n = 4$ for each group). *$P = 0.018$, **$P = 0.05$, and ***$P = 0.02$. Data are plotted as mean ± SD.

Because FGF23 signaling is impaired in *kl/kl* mice, the negative feedback inhibition on vitamin D_3 synthesis is dysfunctional. High vitamin D_3 and phosphate levels in *kl/kl* mice likely stimulate FGF23 synthesis in bone continuously, whereas the elevated PAI-1 levels reduce the proteolytic clearance of FGF23. Together, these combined effects on production, signaling, and metabolism likely explain the >1,200-fold increase in plasma FGF23 levels observed in *kl/kl* mice. Recent reports indicate that dietary deficiency of phosphate, zinc, and calcium significantly improves the lifespan of klotho mice (21, 25, 31). Although we did not detect any significant changes in the levels of phosphate and calcium in *kl/klpai-1*$^{-/-}$ mice, we observed that PAI-1 deficiency significantly prolongs the survival of *kl/kl* mice indicating that, in addition to the mineral homeostasis, PAI-1–regulated extracellular proteolysis strongly influences the aging phenotype.

Our findings also reveal a previously unrecognized role of PAI-1 in modulating the effects of FGF23. The increased plasma levels of PAI-1 in *kl/kl* mice are not surprising, but deserve some mechanistic explanation. Numerous factors likely contribute to the *Klotho* phenotype, and prominent on that list are the effects of TGF-β (16), Wnt (15), and IGF1 (17, 32). Importantly, all three of these factors can directly induce PAI-1 expression. As the phenotype matures, PAI-1 production is likely further augmented by the effects of progressive hypoxemia, the induction of the p53 pathway, aldosterone excess (25), and elevated levels of other components of the SMS, including IL-6, interferons, TGF-β, and IGFBPs.

Discovery of the *Klotho* gene has shed light into the molecular mechanisms of tissue calcification. The elevated phosphate and calcium levels in *kl/kl* mice certainly contribute to the pattern of ectopic calcification (33, 34). Recently, hyperaldosteronism was reported to be the major inducer of the osteog enic signaling, which was partially reversed by spironolactone without normalizing plasma levels of vitamin D_3, FGF23, calcium, and phosphate (24, 25). Furthermore, Lim et al. reported that FGF23 treatment reduced the aldosterone-induced expression of osteogenic factors in vitro (35). In addition, PAI-1 deficiency drastically reduced FGF23 levels and calcification without altering aldosterone and ALP levels in *kl/kl* mice (Table 1). These findings suggest that PAI-1, which is regulated by aldosterone (36), plays an unexpected but pivotal role in tissue calcification. The reduced plasma levels of vitamin D_3 and prevention of tissue calcification in *kl/klpai-1*$^{-/-}$ mice require the restoration of Klotho-independent FGF23 signaling. The present study strongly indicates that PAI-1 plays a direct role in the regulation of FGF23 signaling in *kl/kl* mice.

The reduced IGFBP-3 levels in *kl/kl* mice provide an important mechanistic insight into the protective effects of PAI-1 deficiency on the *Klotho* phenotype. It was recently demonstrated that the PAI-1–IGFBP-3 cascade promotes stress-induced senescence in human breast fibroblasts (37). Expression levels of IGFBP-3 are increased in response to senescence-inducing stimuli. However, the proteolytic metabolism of IGFBP-3 by tissue-type plasminogen activator (t-PA) prevents the induction of cellular

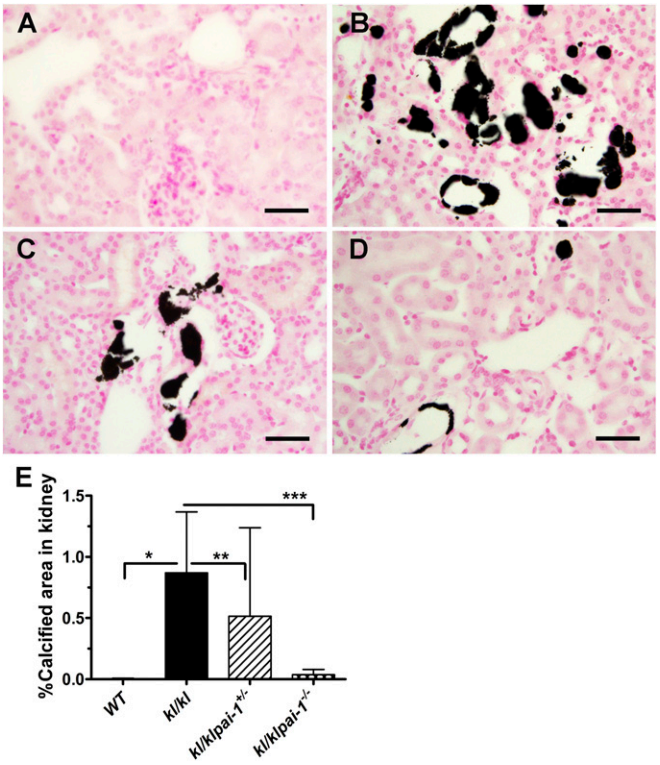

Fig. 5. Effects of PAI-1 deficiency on ectopic calcification characterized by von Kossa staining. Ectopic calcification analysis was performed on kidney ($n = 5$ for each group) sections. Although samples from (*A*) WT mice showed no detectable calcification, kidney sections from (*B*) *kl/kl* mice had remarkable calcified deposits. (*C*) Partial (*kl/klpai-1*$^{+/-}$) or (*D*) complete PAI-1 deficiency (*kl/klpai-1*$^{-/-}$), on the other hand, significantly decreased calcification levels. (Scale bars: 40 μm.) (*E*) Quantitative analyses using Image-Pro-6.3 software showed that the percentages of calcified areas in kidneys were reduced by 41% in *kl/klpai-1*$^{+/-}$ and 96% in *kl/klpai-1*$^{-/-}$ mice compared with *kl/kl* mice. **P* = 0.002, ***P* = 0.03, and ****P* = 0.0001. Data are plotted as mean ± SD.

senescence in vitro. Because PAI-1 is the main physiological inhibitor of t-PA, IGFBP-3 appears to be a critical downstream target of PAI-1–induced senescence. These findings provide a possible mechanistic explanation for the prosenescent effects of increased PAI-1 in *kl/kl* mice and suggest a role for an extracellular cascade of secreted proteins in the regulation of cellular senescence and physiological aging.

It was recently shown that membrane-bound Klotho prevents the retinoic-acid-inducible gene-I–induced expression of IL-6 and -8 both in vitro and in vivo, suggesting that the antiaging function of Klotho also includes the suppression of inflammation (38). It is interesting to note that with PAI-1 deficiency, levels of both IGFBP-3 and IL-6 were normalized in *kl/kl* mice. This confirms and extends the recent observations by López-Andrés et al. that modulating the activity of a key member of the SMS can also normalize the levels of other SMS factors (39). This indicates that IGFBP-3 and IL-6 are downstream from PAI-1 in the senescence pathway.

In human fibroblasts, telomere shortening initiates senescence through a pathway that involves ataxia telangiectasia mutated (ATM), p53, and p21^{CIP1}, but not p16^{Ink4a} (9). Thus, the presence of p16^{Ink4a}-positive but not p21-positive cells in kidneys of *kl/kl* mice suggests that the pathway to senescence and accelerated aging in the renal tissue of *kl/kl* mice is likely mediated by p16^{Ink4a} and occurs independently of the p53 pathway. These findings in the kidney of preserved telomere length, together with augmented p16^{Ink4a} expression, suggest that renal cells undergo senescence without the requisite cellular division to shorten telomeres (22).

The results presented here indicate that PAI-1 is a critical contributor to, and not merely a marker of, senescence in vivo (12), and that novel therapies targeting PAI-1 or other components of the SMS (40) may prevent senescence and age-related pathologic changes in humans, including arteriosclerosis and emphysema. The development of small-molecule, orally active, selective PAI-1 antagonists, such as TM5441 and others (41), will allow these hypotheses to be tested prospectively.

Materials and Methods

Animals and Animal Care. The original genetic background of *kl/kl* mice, a kind gift from Makoto Kuro-o (Jichi Medial University, Shimotsuke, Tochigi, Japan), was composed of C57BL/6J and C3H/J (13). PAI-1–deficient mice were obtained from The Jackson Laboratory (background strain C57BL/6J; strain name B6.129S2-Serpine1tm1Mlg/J; stock no. 002507). *Klotho* mice and PAI-1–deficient mice were crossed to generate the heterozygous dihybrid mice (*KL/kl-pai-1*$^{+/-}$). All mice used in this study were littermates generated by breeding these *KL/kl-pai-1*$^{+/-}$ mice and thus of the same mixed background. They were housed in a temperature-controlled environment with a daily 14:10 h light–dark cycle and had unlimited access to food (standard rodent chow diet; Harlan Teklad) and water. All experimental protocols were approved by the Institutional Animal Care and Use Committee of Northwestern University.

PAI-1 Inhibitor TM5441. TM5441 was derived from the original hit compound TM5007 (42) and the lead compound TM5275 (43) through an extensive structure-activity relationship (44). We have recently described the pharmacokinetic properties and toxicity, and specificity of TM5441 (20). TM5441 was administered at 100 mg/kg·d^{-1} mixed in the chow.

Histological Methods. Tissues harvested from mice were fixed in formalin for 24–48 h and then processed overnight and embedded in paraffin. Tissues sectioned at 6-μm thickness were stained with Masson's trichrome to visualize tissue morphology. Ectopic calcification was analyzed by von Kossa staining of kidneys ($n = 5$ for each study group). The extent of calcification was quantified in multiple kidney sections from each mouse by using Image-Pro-6.3 image-processing software and the results presented as the percent calcified areas in kidneys (Fig. 3). To detect the senescent cells, tissue sections were immunostained overnight at 4 °C with a primary antibody to p16^{Ink4a} antigen (Cell Applications), and then the antigen was visualized with an HRP-conjugated secondary antibody (goat anti-mouse IgG at 1:500 dilution; Santa Cruz Biotechnology, Inc.). One-Step AEC Solution (BioGenex) was used as the substrate for antigen detection.

Quantitation of Factors in Plasma and Serum. Plasma levels of IGFBP-3, IL-6, and FGF23 were measured using the ELISA kits Quantikine Immunoassay kit from R&D Systems (catalog no. MGB300), Becton-Dickinson (catalog no. 555220), and Immutopics (catalog no. 60-6300), respectively, by following the manufacturers' suggested protocols. Vitamin D_3 levels in plasma were measured using the mouse 1,25-$(OH)_2$VitD3 HVD3 ELISA kit from NovaTein Biosciences (catalog no. NB-E20523). Calcium (catalog no. 0150-250), creatinine (catalog no. 0430-120), and phosphate (catalog no. 0830-125) levels were determined by using kits from Stanbio Laboratories. Plasma PAI-1 levels were measured with the Murine PAI-1 Total Antigen Assay from Molecular Innovations. A colorimetric assay kit and an ELISA kit from Abcam were used to measure serum levels of ALP and aldosterone (catalog nos. ab83369 and ab136933, respectively).

Measuring Partial Oxygen Pressure in Arterial Blood. PaO_2 levels in the arterial blood were measured in mice anesthetized with pentobarbital (75 mg/kg body weight, administered i.p.). After adequate anesthesia was achieved, we performed a tracheostomy and sutured a 20-gauge angiocatheter into the trachea. Mice were then placed on a small rodent ventilator (MiniVent; Harvard Apparatus) with the following settings: a respiratory rate of 150 breaths per minute, a tidal volume of 8 mL/kg body weight, and an FiO_2 of 0.21 (room air) as described previously (45). The animals were ventilated for 15 min before a thoracotomy was performed and then 200 μL arterial blood were collected into a heparinized syringe via direct puncture of the left ventricle. The arterial blood sample was processed for gas analysis using the Stat Profile pHOx blood gas analyzer (Nova Biomedical).

Quantitation of ATLR. Genomic DNA isolated from various tissues was used to measure telomere length by qRT-PCR as previously described with minor modification (46, 47). Briefly, telomere repeats were amplified using specially designed primers, which were then compared with the amplification of

a single-copy gene, the 36B4 gene (acidic ribosomal phosphoprotein PO), to determine the ATLR. One hundred nanograms of genomic DNA template were added to each 20 μL reaction containing forward and reverse primers (250 nM each for telomere primers, and 500 nM each for the 36B4 primers), SsoAdvanced SYBR Green Supermix (Bio-Rad USA), and nuclease-free water. A serially diluted standard curve of 100 ng to 3.125 ng per well of template DNA from a WT mouse sample was included on each plate for both the telomere and the 36B4 reactions to facilitate ATLR calculation. Critical values were converted to nanogram values according to the standard curves, and nanogram values of the telomere (T) reaction were divided by the nanogram values of the 36B4 (S) reaction to yield the ATLR. The primer sequences for the telomere portion were as follows: 5′-CGG TTT GTT TGG GTT TGG GTT TGG GTT TGG GTT TGG GTT-3′ and 5′-GGC TTG CCT TAC CCT TAC CCT TAC CCT TAC CCT TAC CCT-3′. The primer sequences for the 36B4 single copy gene portion were as follows: 5′-ACT GGT CTA GGA CCC GAG AAG-3′ and 5′-TCA ATG GTG CCT CTG GAG ATT-3′. Cycling conditions for both primer sets (run in the same plate) were 95 °C for 10 min, 30 cycles of 95 °C for 15 s, and 55 °C for 1 min for annealing and extension.

qRT-PCR. Tissues harvested from subject mice were snap-frozen in liquid nitrogen. Excess tissue was removed under a dissecting microscope. RNA was isolated using the Qiagen RNAeasy Mini Kit (Qiagen) using the manufacturer's protocol. cDNA was generated from the RNA using the qScript cDNA Supermix (Quanta Biosciences). qRT-PCR was performed using the SsoAdvanced SYBR Green Supermix (Bio-Rad USA). Forward and reverse primers used for $p16^{Ink4a}$ expression were, respectively: 5′-AGGGCCGTGTGCATGACGTG-3′ and 5′-GCACCGGGCGGGAGAAGGTA-3′; for PAI-1 expression, respectively: 5′-ACGCCTGGTGCTGGTGAATGC-3′ and 5′-ACGGTGCTGCCATCAGACTTGTG-3′; and for GAPDH expression, respectively: 5′-ATGTTCCAGTATGACTCCACTCACG-3′ and 5′-GAAGACACCAGTAGACTCCACGACA-3′ (IDT, Inc.).

Behavioral Characterization. To test the effect of PAI-1 deficiency on the level of physical activity of *kl/kl* mice, the open field test for spontaneous horizontal activity was performed on age-matched animals at the Northwestern University Mouse Behavioral Phenotyping Core Laboratory as described previously (13).

Statistical Analyses. We present the averaged values obtained for each study as mean ± SD. Statistical significance was assigned to a comparison by using an unpaired, two-tailed Student *t* test when comparing two groups. Statistical significance for the survival of groups was established by the log-rank analysis of Kaplan–Meier plots using GraphPad Prism 4 software. $P < 0.05$ was considered statistically significant.

ACKNOWLEDGMENTS. We thank Dr. Makoto Kuro-o for providing us with the *kl/kl* mice. We also thank Marissa Michaels for her help in obtaining reagents and coordinating various aspects of our projects. This work was supported by National Institutes of Health (NIH)/National Heart, Lung, and Blood Institute Grants 2R01HL051387 and 1P01HL108795. A.T.P. is supported in part by NIH National Institute of Diabetes and Digestive and Kidney Diseases Training Grant T32 KD007169.

1. Rodier F, Campisi J (2011) Four faces of cellular senescence. *J Cell Biol* 192(4):547–556.
2. Campisi J, d'Adda di Fagagna F (2007) Cellular senescence: When bad things happen to good cells. *Nat Rev Mol Cell Biol* 8(9):729–740.
3. Coppé JP, Desprez PY, Krtolica A, Campisi J (2010) The senescence-associated secretory phenotype: The dark side of tumor suppression. *Annu Rev Pathol* 5:99–118.
4. Krtolica A, Parrinello S, Lockett S, Desprez PY, Campisi J (2001) Senescent fibroblasts promote epithelial cell growth and tumorigenesis: A link between cancer and aging. *Proc Natl Acad Sci USA* 98(21):12072–12077.
5. Mu XC, Higgins PJ (1995) Differential growth state-dependent regulation of plasminogen activator inhibitor type-1 expression in senescent IMR-90 human diploid fibroblasts. *J Cell Physiol* 165(3):647–657.
6. Kuilman T, Peeper DS (2009) Senescence-messaging secretome: SMS-ing cellular stress. *Nat Rev Cancer* 9(2):81–94.
7. Dimri GP, et al. (1995) A biomarker that identifies senescent human cells in culture and in aging skin in vivo. *Proc Natl Acad Sci USA* 92(20):9363–9367.
8. Wahl GM, Carr AM (2001) The evolution of diverse biological responses to DNA damage: Insights from yeast and p53. *Nat Cell Biol* 3(12):E277–E286.
9. Herbig U, Jobling WA, Chen BP, Chen DJ, Sedivy JM (2004) Telomere shortening triggers senescence of human cells through a pathway involving ATM, p53, and p21 (CIP1), but not p16(INK4a). *Mol Cell* 14(4):501–513.
10. Serrano M, Lin AW, McCurrach ME, Beach D, Lowe SW (1997) Oncogenic ras provokes premature cell senescence associated with accumulation of p53 and p16INK4a. *Cell* 88(5):593–602.
11. Parrinello S, et al. (2003) Oxygen sensitivity severely limits the replicative lifespan of murine fibroblasts. *Nat Cell Biol* 5(8):741–747.
12. Baker DJ, et al. (2011) Clearance of p16Ink4a-positive senescent cells delays ageing-associated disorders. *Nature* 479(7372):232–236.
13. Kuro-o M, et al. (1997) Mutation of the mouse klotho gene leads to a syndrome resembling ageing. *Nature* 390(6655):45–51.
14. Baker DJ, et al. (2008) Opposing roles for p16Ink4a and p19Arf in senescence and ageing caused by BubR1 insufficiency. *Nat Cell Biol* 10(7):825–836.
15. Liu H, et al. (2007) Augmented Wnt signaling in a mammalian model of accelerated aging. *Science* 317(5839):803–806.
16. Doi S, et al. (2011) Klotho inhibits transforming growth factor-beta1 (TGF-beta1) signaling and suppresses renal fibrosis and cancer metastasis in mice. *J Biol Chem* 286(10):8655–8665.
17. Kurosu H, et al. (2005) Suppression of aging in mice by the hormone Klotho. *Science* 309(5742):1829–1833.
18. Takeshita K, et al. (2002) Increased expression of plasminogen activator inhibitor-1 with fibrin deposition in a murine model of aging, "Klotho" mouse. *Semin Thromb Hemost* 28(6):545–554.
19. Kortlever RM, Higgins PJ, Bernards R (2006) Plasminogen activator inhibitor-1 is a critical downstream target of p53 in the induction of replicative senescence. *Nat Cell Biol* 8(8):877–884.
20. Boe AE, et al. (2013) Plasminogen activator inhibitor-1 antagonist TM5441 attenuates Nω-nitro-L-arginine methyl ester-induced hypertension and vascular senescence. *Circulation* 128(21):2318–2324.
21. Morishita K, et al. (2001) The progression of aging in klotho mutant mice can be modified by dietary phosphorus and zinc. *J Nutr* 131(12):3182–3188.
22. Coviello-McLaughlin GM, Prowse KR (1997) Telomere length regulation during postnatal development and ageing in Mus spretus. *Nucleic Acids Res* 25(15):3051–3058.
23. Suga T, et al. (2000) Disruption of the klotho gene causes pulmonary emphysema in mice. Defect in maintenance of pulmonary integrity during postnatal life. *Am J Respir Cell Mol Biol* 22(1):26–33.
24. Voelkl J, et al. (2013) Spironolactone ameliorates PIT1-dependent vascular osteoinduction in klotho-hypomorphic mice. *J Clin Invest* 123(2):812–822.
25. Fischer SS, et al. (2010) Hyperaldosteronism in Klotho-deficient mice. *Am J Physiol Renal Physiol* 299(5):F1171–F1177.
26. Eren M, Painter CA, Atkinson JB, Declerck PJ, Vaughan DE (2002) Age-dependent spontaneous coronary arterial thrombosis in transgenic mice that express a stable form of human plasminogen activator inhibitor-1. *Circulation* 106(4):491–496.
27. Bernot D, et al. (2011) Plasminogen activator inhibitor 1 is an intracellular inhibitor of furin proprotein convertase. *J Cell Sci* 124(Pt 8):1224–1230.
28. Fukumoto S (2005) Post-translational modification of Fibroblast Growth Factor 23. *Ther Apher Dial* 9(4):319–322.
29. Thomas G (2002) Furin at the cutting edge: From protein traffic to embryogenesis and disease. *Nat Rev Mol Cell Biol* 3(10):753–766.
30. Tian S, Huang Q, Fang Y, Wu J (2011) FurinDB: A Database of 20-Residue Furin Cleavage Site Motifs, Substrates and Their Associated Drugs. *Int J Mol Sci* 12(2):1060–1065.
31. Razzaque MS (2009) The FGF23-Klotho axis: Endocrine regulation of phosphate homeostasis. *Nat Rev Endocrinol* 5(11):611–619.
32. Yamamoto M, et al. (2005) Regulation of oxidative stress by the anti-aging hormone klotho. *J Biol Chem* 280(45):38029–38034.
33. Hu MC, et al. (2011) Klotho deficiency causes vascular calcification in chronic kidney disease. *J Am Soc Nephrol* 22(1):124–136.
34. Ohnishi M, Nakatani T, Lanske B, Razzaque MS (2009) Reversal of mineral ion homeostasis and soft-tissue calcification of klotho knockout mice by deletion of vitamin D 1alpha-hydroxylase. *Kidney Int* 75(11):1166–1172.
35. Lim K, et al. (2012) Vascular Klotho deficiency potentiates the development of human artery calcification and mediates resistance to fibroblast growth factor 23. *Circulation* 125(18):2243–2255.
36. Brown NJ, et al. (2000) Aldosterone modulates plasminogen activator inhibitor-1 and glomerulosclerosis in vivo. *Kidney Int* 58(3):1219–1227.
37. Elzi DJ, et al. (2012) Plasminogen activator inhibitor 1—insulin-like growth factor binding protein 3 cascade regulates stress-induced senescence. *Proc Natl Acad Sci USA* 109(30):12052–12057.
38. Liu F, Wu S, Ren H, Gu J (2011) Klotho suppresses RIG-I-mediated senescence-associated inflammation. *Nat Cell Biol* 13(3):254–262.
39. López-Andrés N, et al. (2013) Absence of cardiotrophin 1 is associated with decreased age-dependent arterial stiffness and increased longevity in mice. *Hypertension* 61(1):120–129.
40. Peeper DS (2011) Ageing: Old cells under attack. *Nature* 479(7372):186–187.
41. Tashiro Y, et al. (2012) Inhibition of PAI-1 induces neutrophil-driven neoangiogenesis and promotes tissue regeneration via production of angiocrine factors in mice. *Blood* 119(26):6382–6393.
42. Izuhara Y, et al. (2008) Inhibition of plasminogen activator inhibitor-1: Its mechanism and effectiveness on coagulation and fibrosis. *Arterioscler Thromb Vasc Biol* 28(4):672–677.
43. Izuhara Y, et al. (2010) A novel inhibitor of plasminogen activator inhibitor-1 provides antithrombotic benefits devoid of bleeding effect in nonhuman primates. *J Cereb Blood Flow Metab* 30(5):904–912.
44. Miyata T, Yamaoka N, Kodama H, Murano K (2011) Inhibitor of plasminogen activator inhibitor-1. US Patent Appl 2,011,112,140 A1 (May 12, 2011).
45. Mutlu GM, et al. (2004) Upregulation of alveolar epithelial active Na+ transport is dependent on beta2-adrenergic receptor signaling. *Circ Res* 94(8):1091–1100.
46. Cawthon RM (2002) Telomere measurement by quantitative PCR. *Nucleic Acids Res* 30(10):e47.
47. Callicott RJ, Womack JE (2006) Real-time PCR assay for measurement of mouse telomeres. *Comp Med* 56(1):17–22.